

## OXIDE SCALE FORMATION IN NOVEL $\gamma$ - $\gamma'$ COBALT-BASED ALLOYS

C.A. Stewart<sup>1</sup>, R.K. Rhein<sup>1</sup>, A. Suzuki<sup>2</sup>, T.M. Pollock<sup>1</sup>, C.G. Levi<sup>1</sup>

<sup>1</sup>Materials Department, University of California, Santa Barbara, CA 93106-5050, USA

<sup>2</sup>GE Global Research, One Research Cr.; Niskayuna, NY, 12309, USA

Keywords: Cobalt alloys, Oxidation, Combinatorial study

### Abstract

Oxidation behavior has been investigated for three cast novel Co-base  $\gamma$ - $\gamma'$  alloys and a subset of alloys produced by combinatorial ion plasma deposition exploring the effect of Ni:Co ratio and Al content. Oxidation was performed at 1100 °C for 1 h in flowing dry air; the oxide scale was characterized by luminescence spectroscopy and scanning electron microscopy (SEM) with energy dispersive spectroscopy (EDS). First-principles thermodynamic modeling of Co-Ni-W-Al-Cr-Ta-O compositions predicts  $\alpha$ -Al<sub>2</sub>O<sub>3</sub> for all two-phase  $\gamma$ - $\gamma'$  alloys, but alumina may often form internally as discrete particles rather than as a continuous surface scale. Experimental assessment of  $\alpha$ -Al<sub>2</sub>O<sub>3</sub> scale formation by combinatorial synthesis suggests that minimum levels of Al and Ni:Co are needed, but the effect of the Ni:Co ratio is likely modest above the critical Al content.

### Introduction

Nickel-base superalloys have long been the enabling material in advancing gas turbine technology but are generally considered to be reaching a fundamental limit to their capability as the solvus temperature of  $\gamma'$  approaches the solidus [1, 2]. Persistent demands for higher fuel efficiency and concomitant increases in the component operating temperatures motivate the search for alternate structural materials for the hot gas path. Co-W-Al based alloys discovered within the last decade [3] exhibit  $\gamma$ - $\gamma'$  microstructures at 900 °C similar to those characteristic of current Ni-based superalloys. These new Co-base alloys have attractive properties including solidus temperature 100 °C - 150 °C higher than those of commercial alloys such as CMSX-4 [2, 4], as well as a 0.2 % flow stress exceeding that of Ni-base superalloys above 900 °C [5]. In addition, the Co-W-Al based alloys exhibit reduced segregation of Al and W during solidification, suggesting resistance to convective instabilities and freckle formation [6].

As modern superalloys are able to maintain adequate creep resistance at temperatures approaching 1100 °C [7], competitive Co-base  $\gamma$ - $\gamma'$  alloys must be developed to have both superior mechanical properties, usually linked to a suitably high  $\gamma'$  solvus temperature, as well as a modicum of intrinsic oxidation resistance. The rationale for the latter requirement is the potential loss or damage of the anticipated thermal barrier coating system that may expose the structural alloy to the chemically aggressive environment within the gas turbine [8]. Desirable oxidation resistance at the temperatures of interest is optimally imparted by the formation of an external  $\alpha$ -Al<sub>2</sub>O<sub>3</sub> scale. The latter is not only more thermodynamically stable, a better oxygen diffusion barrier which leads to slower growth, and essentially non-volatile in high temperature water vapor in comparison with the chromia scales formed in previous generations of Co-base superalloys [9, 10]. In assessing the effects of alloying additions to the Co-W-Al  $\gamma$ - $\gamma'$  system it is important to consider the potential synergism or trade-

off between the effects on the  $\gamma'$  stability and on the formation of the  $\alpha$ -Al<sub>2</sub>O<sub>3</sub> scale at the target temperatures, nominally  $\geq$  1100 °C. For example, previous studies have shown that B and Cr benefit the oxidation resistance [1, 11], but Cr also depresses the  $\gamma'$  solvus [1, 2]. It is generally accepted that the  $\gamma$ + $\gamma'$  field in the ternary Co-W-Al system is quite small at 900 °C and is not present at 1000 °C [3]. Therefore, alloying additions are necessary to stabilize the  $\gamma'$  phase at the temperatures of interest. Notable amongst them is Ni, which considerably increases the size of the  $\gamma$ + $\gamma'$  field at 900 °C [12]. It has also been shown that modest amounts (2 at. %) of Ta and Ti increase the  $\gamma'$  solvus by 82 °C and 60 °C respectively [13].

Formation of an external Al<sub>2</sub>O<sub>3</sub> scale in Co-base  $\gamma$ - $\gamma'$  alloys has been reported by various authors [1, 4, 11, 14], but such a scale is typically convoluted, overlaid by 10-100  $\mu$ m of non-protective oxides, and is often accompanied by changes in the composition of the underlying alloy to yield the undesirable topologically close packed Co<sub>3</sub>W phase. While some amount of overlying non-protective oxides may be acceptable locally on surfaces exposed to the environment by coating damage or loss, the oxidation rate should still proceed slowly to ensure that the mechanical integrity of the component is retained until a scheduled inspection can detect the damage. This could typically involve times of thousands of hours, with scale thicknesses limited to  $\sim$ 10  $\mu$ m. One of the most oxidation resistant  $\gamma$ - $\gamma'$  Co alloys reported is Co-7Al-7W-10Cr (in at. %), which forms  $\sim$ 1.3  $\mu$ m of oxide scale after 196 h cyclic oxidation at 800 °C [1]. Unfortunately, most investigations into the oxidation resistance of Co alloys have been performed between 800 °C - 1000 °C, well below the desired target of 1100 °C for  $\gamma$ - $\gamma'$  Co alloys that are also protective  $\alpha$ -Al<sub>2</sub>O<sub>3</sub> formers. Furthermore, it would be advantageous for such an alloy to generate continuous alumina scale in short times, of order 1 h, to minimize the growth of overlying oxides or excessive Al depletion below the scale.

The work reported here is part of a broader investigation on the effects of alloying on the oxidation resistance and  $\gamma'$  solvus temperature for the novel family of  $\gamma$ - $\gamma'$  Co alloys. First principles thermodynamic modeling has been employed for investigation of stable oxide phases. To broadly explore the multidimensional compositional space for  $\alpha$ -Al<sub>2</sub>O<sub>3</sub> formation, a combinatorial synthesis approach has been undertaken. Sample libraries with variations in Co, Ni, Al, W, and Cr have been synthesized by ion plasma deposition. The feasibility of Co-base alloys with the desirable combinations of properties at 1100 °C is assessed.

### Experimental Methods

Three exploratory Co-base alloys with the compositions shown in Table I were investigated. These alloys contain more than 7 at. % Cr for improving environmental resistance and high amount of Ni and Ta to achieve solvi temperatures higher than 1000 °C.

Table I: Cast Alloy Compositions in Atomic %, and  $\gamma'$  Solvi as Measured by Dilatometry.

Alloy	Co	Ni	Al	W	Cr	Ta	C	B	Y	Mo	$\gamma'$ Solvus
Co-1	43.61	27.41	8.82	5.60	12.37	1.88	0.27	0.03	0	0	1035 °C
Co-2	42.84	30.08	8.64	5.44	8.97	3.68	0.28	0.03	0.04	0	1118 °C
Co-3	42.37	32.00	8.55	5.56	7.60	2.55	0.27	0.03	0.04	1.03	1090 °C

Alloy Co-1 serves as a baseline, with alloys Co-2, and 3 having only moderate variations in the contents of the major components but containing small amounts of additional Y, and Y+Mo respectively. All alloys were vacuum induction melted and subsequently solution heat treated at 1200 °C for 4 h and aged at 950 °C for 50 h. Sample buttons were electro-discharge machined from the ingots of the three alloys in Table I, as well as from a René N5 single crystal for comparison. The buttons were approximately 15.5 mm in diameter by 2.5 mm in height, polished to 800 grit finish, and ultrasonically cleaned for 20 minutes in acetone followed by 20 minutes in isopropanol prior to oxidation.

A set of combinatorial libraries were designed and synthesized by ion plasma deposition (IPD) [15] to explore systematically the effects of composition on the oxidation behavior of  $\gamma$ - $\gamma'$  alloys. Each library consisted of a triangular array of 78 buttons arranged beneath three cathode sources at the corners, each with one of the compositions listed in Table II. All cathode sources contained the baseline ternary elements Co-W-Al, as well as Cr (to enhance oxidation resistance) and Ta (to increase the  $\gamma'$  solvus). Except for Cathode 1, all others also contained Ni, known to expand the  $\gamma$ - $\gamma'$  field. Cathodes 1 and 2 were used in all three combinatorial libraries to explore the changes in the Ni:Co ratio. Each library was then distinguished by the third cathode, designed to provide a varying concentration of Cr (3), W (4), or Al (5). This paper reports preliminary results on the library formed by cathodes 1, 2 and 5, with the remaining studies to be published at a later date.

Alloy compositions were deposited on buttons with composition nominally corresponding to Cathode 1 to minimize the interdiffusion with the deposited alloy. Each button was approximately 12.7 mm in diameter by 2.5 mm in height. The button centers were separated by approximately 20 mm from their nearest neighbors, and the cathodes were centered over the corners of the library at distances between centers of approximately 163 mm. In the present case, each button in a given combinatorial library had a coating of a composition varying systematically between those of the cathode sources, depending on its position in the array. The compositions of these coatings were selected to represent a range of potential structural alloys, not bond coats suitable for subsequent deposition of thermal barrier coatings.

Table II: Compositions of the Cathode Sources Used for Creation of the Three Combinatorial Libraries\*

	Co (at. %)	Ni (at. %)	W (at. %)	Al (at. %)	Cr (at. %)	Ta (at. %)	S (ppmw)	Ni:Co (at.)
Substrate	79.7	0.0	6.7	8.9	3.3	1.5	0.5	0:1
Cathode 1	77.1	0.0	5.9	12.2	3.4	1.4	3	0:1
Cathode 2	33.5	35.4	11.8	14.4	3.4	1.5	2	1:1
Cathode 3	30.0	29.3	6.0	11.8	21.5	1.4	4	1:1
Cathode 4	40.9	40.4	0.0	13.8	3.5	1.4	1	1:1
Cathode 5	33.4	34.6	6.5	20.7	3.4	1.4	1	1:1

\* Compositions measured by ICP, with sulfur content in parts per million by weight. Cathodes 1 and 2 were used in all three libraries, and the library discussed in the present study was created of cathodes 1, 2, 5.

Furthermore, the target coating thickness was 150  $\mu\text{m}$ , such that the layer is thick enough to represent bulk alloy oxidation behavior. To reduce the alloy heterogeneity inherent to the deposition process, all buttons were solution heat treated in vacuum at  $\sim 1200$  °C, above the highest estimated  $\gamma'$  solvus, and then polished with 0.05  $\mu\text{m}$  colloidal alumina. No aging treatment was provided as  $\gamma'$  would be expected to precipitate in heating to the oxidation temperature. The surface compositions of the heat-treated buttons were then measured for selected specimens by SEM EDS. The analysis was conducted on an approximately 1 mm<sup>2</sup> subsection of the button surfaces at an accelerating voltage of 15 kV. The prepared buttons of the three exploratory alloys, René N5, and the combinatorial samples were oxidized at 1100 °C in flowing dry air within a tube furnace. To conduct oxidation tests, sample buttons were inserted into the hot zone of the furnace previously heated to the prescribed temperature and with the established controlled atmosphere, held for the prescribed time, and then withdrawn from the furnace over the course of 2 minutes. Any spalled oxidation products were not recovered from the sample holder. Buttons of the three exploratory alloys and René N5 were initially oxidized for 1 hour, and subsequent samples of Co-1 were polished with 0.05  $\mu\text{m}$  colloidal alumina and oxidized for a series of shorter times ranging from 3 minutes to 1 hour. All combinatorial buttons were oxidized for 1 hour.

The oxide scales were initially analyzed non-destructively by luminescence spectroscopy using a Horiba LabRam Aramis spectrometer with 633 nm incident laser. Spectra were taken at several points over the oxidized surface of the buttons to determine the presence or absence of the characteristic  $\alpha$ -Al<sub>2</sub>O<sub>3</sub> fluorescence doublet at 14400 cm<sup>-1</sup> [16]. Non-protective, typically discontinuous alumina formed internally within the opaque alloy would not be detectable by this method, so a positive signal would confirm the presence of  $\alpha$ -Al<sub>2</sub>O<sub>3</sub> on the surface. Thus, luminescence spectroscopy offers a rapid-screening technique to identify alumina-forming regions within the library of investigated compositions, and allows faster sample throughput than a technique such as X-ray diffraction.

To verify the results of the luminescence spectroscopy screening, oxidized samples of René N5 and the three cast alloys were analyzed in cross-section using backscattered electron imaging and EDS in the SEM. To prepare samples for microscopy, oxidized buttons were embedded in epoxy, cross-sectioned, and polished to a 0.05  $\mu\text{m}$  colloidal alumina finish. Some samples were noted to have friable oxide scale, and were first plated with a commercial electroless Ni plating solution prior to mounting in epoxy and cross-sectioning. Unless otherwise noted, samples should be assumed to have been mounted in epoxy without Ni plating. The accelerating voltage used for EDS analysis of the cross-sections was 10 kV to reduce the electron interaction volume and sample drift. The drawback of this approach is that the voltage was not energetic enough to differentiate between W and Ta signals.

### Computational Methods

The thermodynamic stability of all existing crystal structures were analyzed for all binary and ternary intermetallics in the Co-Al-W and Ni-Al-W systems using density functional theory (DFT). These calculations were performed using the plane-wave pseudopotential-based Vienna *ab initio* simulation package (VASP) [17,18]. The plane-wave basis set is a common DFT technique used to increase computational efficiency by allowing for faster switching between real and reciprocal space calculations. The use of a pseudopotential also increases computational efficiency by approximating the effects of core electrons. The Perdew, Burke, and Ernzerhof (PBE) general gradient approximation was used for the exchange and correlational functional [18-20]. All structures were allowed to relax to equilibrium and k-point convergence tests were conducted. Formation energies were assessed at 0 K relative to the pure elements in their ground states. In addition, the formation energies of  $\alpha\text{-Al}_2\text{O}_3$  and other oxides relevant to the current Co-base alloys were obtained from the Materials Project database [21]. The oxide formation energies,  $g$ , were then modified to obtain a new characteristic potential,  $\phi$ ,

$$\phi = g - \mu_{\text{O}}N_{\text{O}} \quad (1)$$

where  $\mu_{\text{O}}$  is the oxygen chemical potential and  $N_{\text{O}}$  is the number of oxygen atoms in the chemical formula. This new potential was minimized at increasing oxygen chemical potentials to assess the most thermodynamically stable sequence of oxide formation for several Co-Ni-W-Al-Cr-Ta compositions.

### Results

#### Cast Alloys:

All three exploratory cast alloys were polycrystalline, with average grain sizes of approximately 50-250  $\mu\text{m}$ . They also exhibited a W/Ta-rich carbide phase in addition to  $\gamma$  and  $\gamma'$  phases (Figure 1). The luminescence spectra for the oxide scales on the three exploratory alloys and René N5 are presented in Figure 2. The scale on the exploratory Co alloys spalled to different degrees, presumably during cooling from the oxidation temperature, so multiple luminescence spectra were taken at different points across the surface of the samples. These data show that while single crystal René N5 oxidized under the given conditions exhibits the characteristic  $\alpha\text{-Al}_2\text{O}_3$  doublet, the three cast Co alloys do not show a comparable luminescence signal, with the exception of local areas in Co-3.

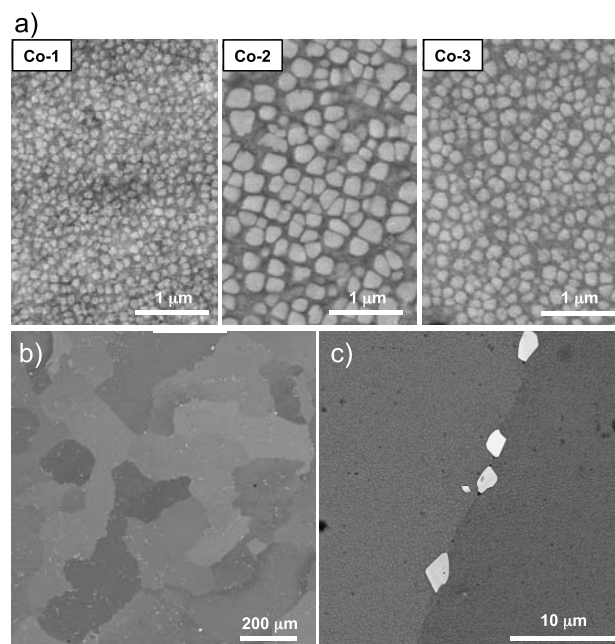
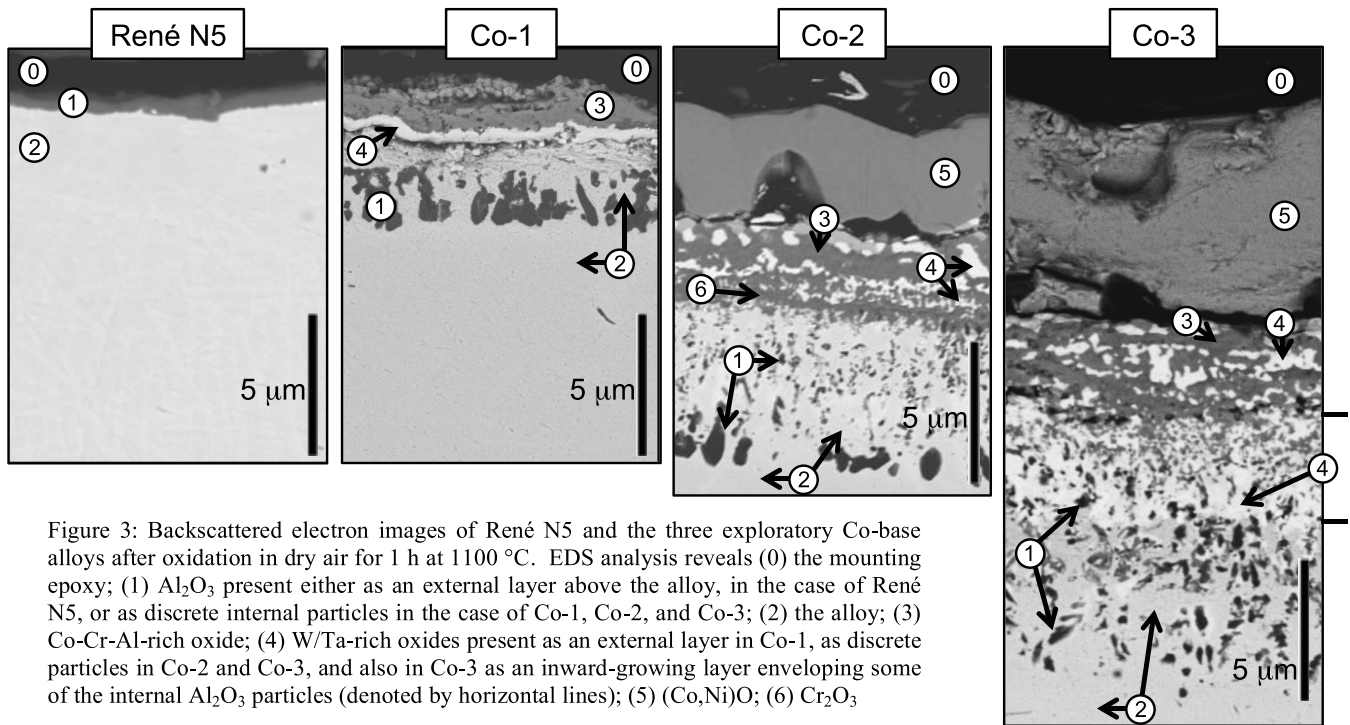
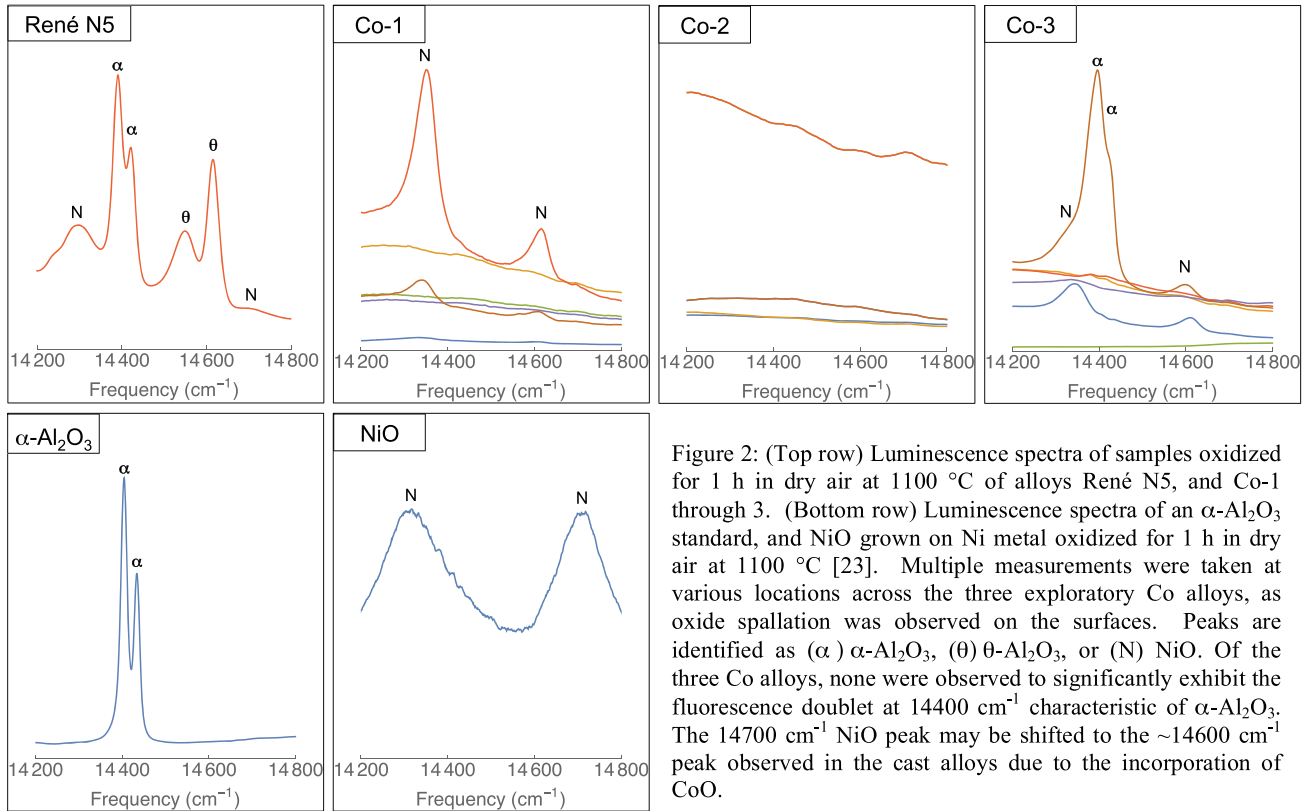


Figure 1: Backscattered electron images of (a) the  $\gamma$ - $\gamma'$  microstructure for the three exploratory alloys, (b) the polycrystalline structure of Co-2, and (c) W/Ta-rich carbides in Co-2.

Of the samples analyzed in cross section, only the René N5 alloy formed external alumina scale after 1 h (Figure 3). The cast Co alloys exhibit discrete alumina particles within a metal matrix, forming an internal oxidation zone (IOZ). The IOZ depth varies between cast alloys, with Co-1 having the thinnest, of approximately 3  $\mu\text{m}$ . Additionally, segmentation of the IOZ of Co-1 via ImageJ reveals an area fraction of approximately 47 % alumina. Lastly, the IOZ of the Co-3 sample consists of discrete alumina particles contained both within the alloy towards the interior, as well as alumina particles enveloped within an inward-growing oxide layer closer to the exterior of the sample. Spallation is frequently observed at the top interface of this layer of alumina particles in oxide, exposing them to the surface. This potentially explains the occasional  $\alpha\text{-Al}_2\text{O}_3$  doublet observed on the Co-3 sample despite the lack of external alumina scale, as these alumina particles in the spalled regions would be exposed to the spectrometer laser.

Chemical analysis of the oxide phases via EDS reveals that the outer layer oxide in Co-2 and Co-3 consists of Ni and Co (Figure 3). This layer is likely a solid solution  $(\text{Co,Ni})\text{O}$ , as CoO and NiO are mutually soluble at the test temperature 1100  $^{\circ}\text{C}$  [22]. SEM analysis of oxidized sample surfaces before cross-sectioning revealed outer  $(\text{Co,Ni})\text{O}$  scale also present on the surface of the Co-1 alloy on some portions of the button. Under this  $(\text{Co,Ni})\text{O}$  layer, Co-1 appears to contain a Co-Cr-Al-O layer, with an underlying W/Ta-rich scale, and lastly the IOZ consisting of discrete alumina particles within the metal matrix (Figure 3). The layers below  $(\text{Co,Ni})\text{O}$  in Co-2 appear to be particles of W/Ta-rich oxide interspersed with Co-Cr-Al-O, followed by chromia, and lastly internal alumina particles within the metal. Oxide scale below  $(\text{Co,Ni})\text{O}$  in the Co-3 sample consists of Co-Cr-Al-O interspersed with particles of W/Ta-rich oxide, followed by the IOZ. However, the upper portion of the Co-3 IOZ is contained within an inward-growing W/Ta-rich oxide, with the bottom portion of the IOZ inside the metal (Figure 3).



## Baseline Alloy

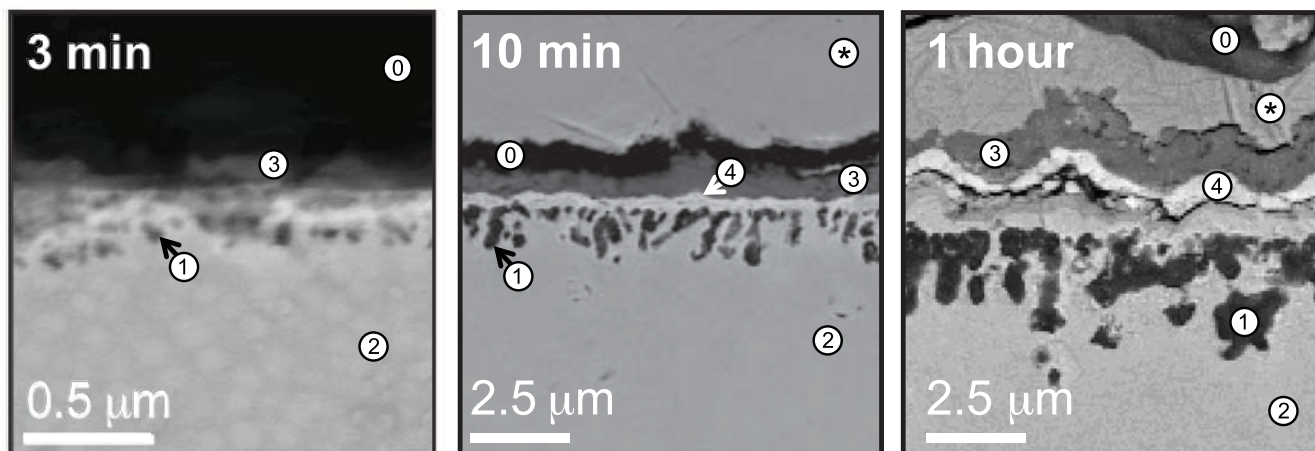


Figure 4: Backscattered electron images depicting the evolution of oxide scale formed on the baseline Co-1 alloy between 3 minutes and 1 hour. All three samples were polished with 0.05  $\mu\text{m}$  colloidal alumina prior to oxidation. EDS analysis reveals (\*) Ni plating; (0) the mounting epoxy; (1)  $\text{Al}_2\text{O}_3$  particles observed to initially nucleate internally within the alloy matrix by 3 minutes; (2) the alloy; (3) non-protective Co-containing oxide scale also formed by 3 minutes; (4) W/Ta-rich oxide scale formed between 3 and 10 minutes.

Additional buttons of Co-1 oxidized for times of 3 minutes, 10 minutes, and 1 h were used to further define the order of formation for the various features (Figure 4). In this series, discrete alumina particles nucleate internally within the metal matrix, and external non-protective scales have already formed by 3 minutes. Over time, the alumina particles coarsen while the IOZ grows deeper into the alloy, and the W/Ta-rich oxide scale develops by 10 minutes. No additional oxide phases were observed to form between 10 minutes and 1 hour.

### Combinatorial Alloys:

The combinatorial IPD synthesis resulted in buttons with relatively thick coatings, approximately 115  $\mu\text{m}$  after deposition. The as-deposited coatings contained some porosity amongst a somewhat compositionally heterogeneous splat-like microstructure, Figure 5(a). Approximately 100  $\mu\text{m}$  of the original coating thickness remained after the development of the interdiffusion zone associated with the solution heat treatment, and the removal of material during polishing of the button surfaces. The average grain size in the heat treated coatings was approximately 7  $\mu\text{m}$ , Figure 5(b). The compositions of the combinatorial buttons as measured by SEM EDS (Table III) vary significantly from those that may be calculated from the cathode sources (Table II). The implication is that the transfer functions for these alloys need to be refined for improved prediction of the composition boundaries. Nevertheless, the resulting combinatorial samples do systematically explore an adequate compositional range for the desired oxidation studies, as illustrated in Figure 6.

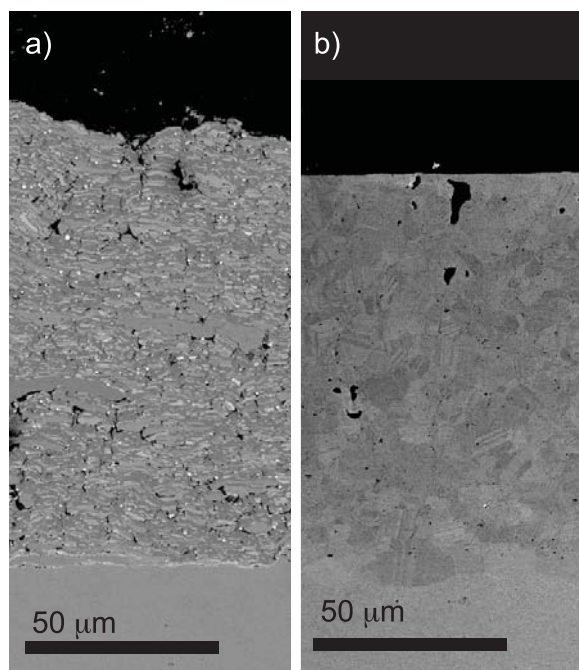


Figure 5: Backscattered electron images of the combinatorial coating on top of substrate button 3-1A (Figure 6) in cross-section after deposition (a), and after solution heat treatment and surface polishing (b).

Luminescence spectroscopy of oxidized buttons along the boundaries of the combinatorial library, shown in Figure 7, revealed both samples with and without the characteristic  $\alpha\text{-Al}_2\text{O}_3$  signal. Buttons in Figure 7 are colored green if the alumina doublet was detected in the spectrum, and red if it was not. Of the buttons tested so far there appears to be a large region of the library where samples display the  $\alpha\text{-Al}_2\text{O}_3$  doublet. This region encompasses compositions higher in Al as well as in Ni:Co ratio, i.e. originating at the boundary between cathodes 2 and 5. At the other end, close to cathode 1, the characteristic alumina doublet is consistently absent.

The transition between the regions where  $\alpha\text{-Al}_2\text{O}_3$  is detected by luminescence and those in which it is not is located approximately along the bounding line between buttons 3-1E and 3-1F, 3-4C and 3-4D, and 3-5A and 3-6A. Comparing the SEM EDS chemical analysis of the unoxidized 3-1E, 3-1F, 3-4C, 3-4D, and 3-5A samples reveals that this transition occurs approximately along a

constant Al concentration, ~10.4 at. % and a concomitant Ni:Co ratio of ~0.46, Figure 6. The extent of coupling between the Al content and Ni:Co ratio in the formation of the  $\alpha$ -Al<sub>2</sub>O<sub>3</sub> scale, however, can not be elucidated from the results available at this time, since all specimens with higher Al content also have similar

or higher Ni:Co ratio. Oxidation of the remaining buttons and subsequent cross-sectioning and compositional analysis are in progress to define more accurately the boundary between the alumina forming and non-forming domains, and to assess the effects of Al and Ni:Co on oxidation behavior individually.

Table III: Select Compositions of Unoxidized Combinatorial Buttons After Solution Heat Treatment and Polishing<sup>§</sup>

Button	Co (at. %)	Ni (at. %)	W (at. %)	Al (at. %)	Cr (at. %)	Ta (at. %)	Ni:Co (at.)
3-1B	65.8	11.2	9.4	7.7	2.3	3.6	0.17
3-1D	60.0	16.2	9.7	8.6	1.7	3.9	0.27
3-1E <sup>†</sup>	55.0	20.1	9.6	9.9	1.8	3.6	0.37
3-1F*	51.1	23.3	9.7	10.5	1.7	3.7	0.46
3-1H	41.7	31.9	10.1	11.3	1.6	3.5	0.77
3-1J	38.3	35.2	10.0	11.4	1.4	3.8	0.92
3-1L	35.5	37.6	10.1	11.3	2.3	3.3	1.06
3-4C <sup>†</sup>	54.4	20.4	9.2	10.3	2.1	3.5	0.37
3-4D*	51.2	24.1	8.9	10.4	1.7	3.6	0.47
3-5A <sup>†</sup>	57.7	18.0	9.5	9.8	1.2	3.8	0.31
3-12A	37.9	34.5	7.1	15.5	1.9	3.0	0.91

<sup>§</sup> Compositions as measured by SEM EDS.

\* Denotes buttons along likely alumina-forming boundary which display the characteristic  $\alpha$ -Al<sub>2</sub>O<sub>3</sub> doublet

<sup>†</sup> Denotes buttons along likely alumina-forming boundary without an  $\alpha$ -Al<sub>2</sub>O<sub>3</sub> doublet

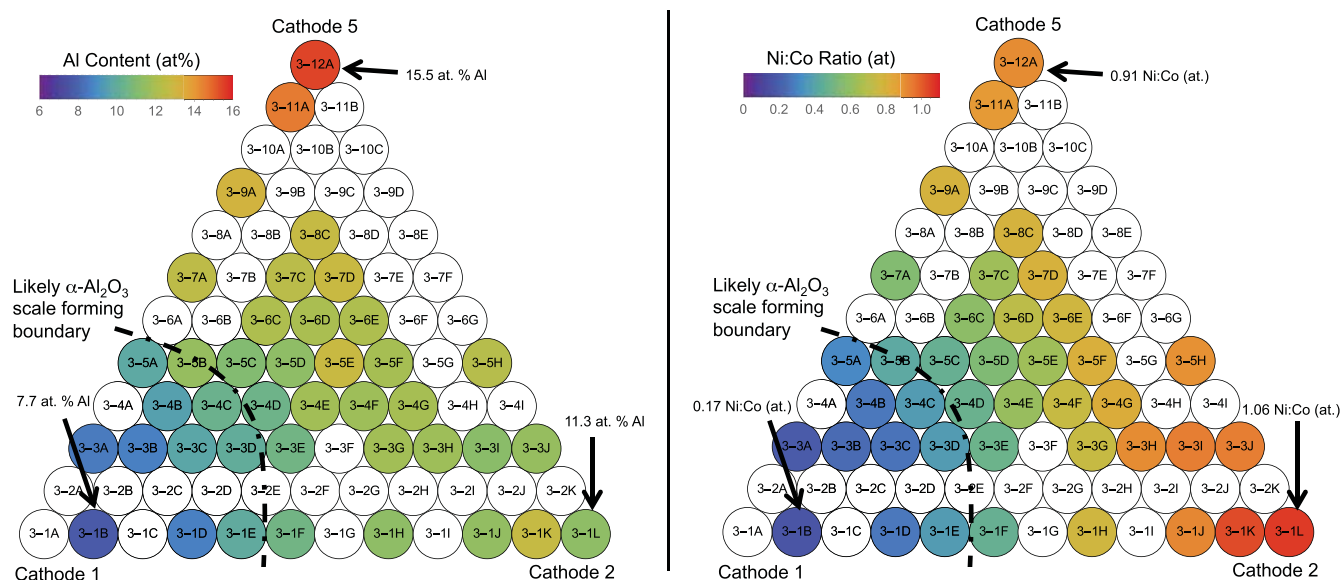


Figure 6: Diagrams of relative positions of combinatorial buttons in the present library, colored based on the concentrations of Al and Ni:Co ratio for select buttons after solution heat treatment and polishing as measured by SEM EDS. Compositional gradients are visible, as Al content increases primarily vertically across the library, while Ni:Co ratio increases primarily horizontally across the library. Buttons in white remain under investigation. (The PDF of the manuscript on the Conference CD shows color images.)

#### Thermodynamic Assessment:

To provide insight into the sequence of formation of the thermodynamically favorable oxides in the scale, first principles calculations were performed for select combinatorial buttons in the senary Co-Ni-W-Al-Cr-Ta system representing the approximate corners of the combinatorial library in Figure 7, i.e. 3-1B, 3-1L and 3-12A. Amongst all the oxide compounds considered,  $\alpha$ -Al<sub>2</sub>O<sub>3</sub> has the largest formation energy at 0 K, viz. -3.44 eV/atom. As the prescribed oxygen chemical potential was gradually increased, the first oxide compound to come into

stable thermodynamic equilibrium with the alloy composition was  $\alpha$ -Al<sub>2</sub>O<sub>3</sub> for all compositions of interest. This is driven by the superior stability of  $\alpha$ -Al<sub>2</sub>O<sub>3</sub> and the concomitantly low aluminum content in the alloy required to form this oxide. As the chemical potential is allowed to increase further, the sequence of thermodynamically favorable oxides was found to be AlTaO<sub>4</sub>, Cr<sub>2</sub>O<sub>3</sub>, spinel CoCr<sub>2</sub>O<sub>4</sub>, and spinel CoAl<sub>2</sub>O<sub>4</sub> for the three button compositions calculated (Figure 8). Beyond CoAl<sub>2</sub>O<sub>4</sub>, the scale layering differs among the three compositions. While all contain CrWO<sub>4</sub>, CoTa<sub>2</sub>O<sub>6</sub>, CoCr<sub>2</sub>O<sub>4</sub> returning to equilibrium at higher oxygen potential, and CoO,

only the 3-1B and 3-12A compositions were predicted to contain  $\text{CoWO}_4$ , and only 3-1B was calculated to contain  $\text{WO}_2$ . Furthermore, the location of the  $\text{CoTa}_2\text{O}_6$  layer in the stack differs for the 3-12A composition, where it is calculated to lie below the  $\text{CrWO}_4$  layer. With even greater oxygen potentials, the spinel  $\text{Co}_3\text{O}_4$  is predicted to become stable, and even higher

oxygen potentials are needed before the Ni oxides are stabilized (not shown). It is noted that no solid solubility is allowed in these calculations as implied by the 0 K temperature. A significant implication is that layers with the same structure are immiscible, e.g. the spinels  $\text{CoAl}_2\text{O}_4$  and  $\text{CoCr}_2\text{O}_4$ , and presumably the  $\text{Co}_3\text{O}_4$  expected above  $\text{CoO}$ .

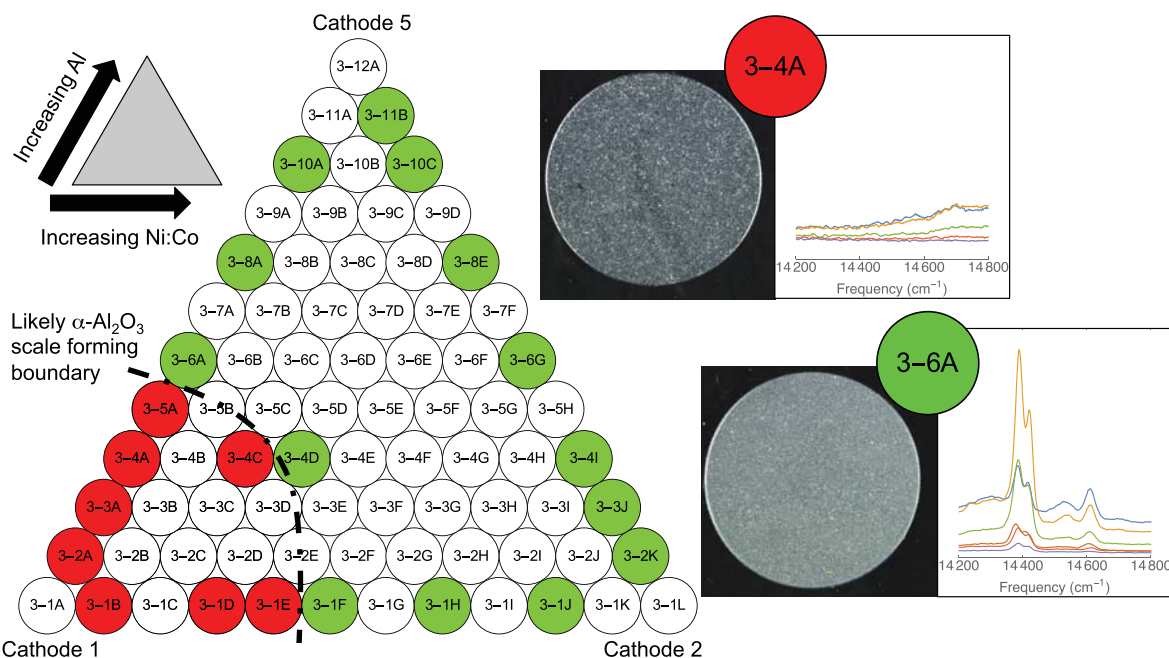


Figure 7: Diagram of the relative positions of combinatorial buttons in the library investigating changing Ni:Co (horizontally), and Al content (vertically). Cathode sources 1, 2, and 5 in Table II used for synthesis of the shown samples were centered over buttons 3-2B, 3-2J, and 3-10B respectively. Buttons are labeled based on their position within the library, and colored based on the detection (green) or absence (red) of the characteristic  $\alpha\text{-Al}_2\text{O}_3$  fluorescence doublet (right). Buttons in white remain under investigation. Select measurements of unoxidized sample compositions are listed in Table III. All buttons were oxidized in flowing dry air for 1 h at 1100 °C. (The PDF of the manuscript on the Conference CD shows color images.)

## Discussion

The results of the 1 h oxidation tests of the three exploratory cast Co alloys do not reveal formation of a continuous alumina scale for any of the three alloys, containing between 8.55 and 8.82 at. % of Al. However, the Co-1 alloy has an internal alumina volume fraction  $f_v \approx 0.47$ . This value is relatively high when compared with the few available quantified critical oxide volume fractions necessary for external scale formation ( $f_v^*$ ), of 0.3 and 0.5 for Ag-In and Fe-Si, respectively [24]. Furthermore, the measured  $\gamma'$  solvi of the three cast alloys approach the nominal temperature range of interest, > 1100 °C. These results suggest that with proper selection of alloying additions, e.g. [1, 11, 13], it should be possible to design a multicomponent Co-base  $\gamma\text{-}\gamma'$  alloy that forms an external  $\alpha\text{-Al}_2\text{O}_3$  scale and has a  $\gamma'$  solvus comparable to, or exceeding that of, Ni-base superalloys for the envisaged applications. Yet, based on the results from the cast alloys, which all exhibit internal oxidation, it is evident that achieving the combination of goals above is non-trivial.

To help identify the conditions under which alumina scale is achievable for  $\gamma\text{-}\gamma'$  Co alloys, it would be desirable to model both the thermodynamics and the kinetics of the oxidation reactions. First principles calculations (at 0 K) indicate that the  $\alpha\text{-Al}_2\text{O}_3$  is thermodynamically the most stable oxide. However, a large

number of stable Co-containing oxides are also expected at higher oxygen potentials, resulting in non-protective outer layers. With regard to kinetics, current modeling approaches, mostly based upon Wagner's analysis [24-26], have typically addressed only binary or ternary systems, and the accuracy of such models varies greatly between material systems.

In light of these modeling limitations, an experimental approach based on the synthesis of combinatorial libraries is being used to explore the composition space where alumina scales may be formed by Co-base  $\gamma\text{-}\gamma'$  alloys, and how systematic changes in composition affect the ability of Co alloys to form alumina scale. Current results indicate that compositions of  $x\text{Co-yNi-10W-zAl-2Cr-3.5Ta}$  at. %, where the ratio  $y/x$  is at least 0.46, and  $z$  is at least 10.4 at. % are likely to yield alumina scales upon oxidation at 1100 °C. Note, however, that the small grain size of the combinatorial buttons likely benefits alumina formation, and thus the Al content necessary for external scale formation after short times is likely higher at larger grain sizes. In the context of these combinatorial results, all three cast alloys have Al contents somewhat below 10.4 at. %, as shown in Table I, the minimum amount necessary for detectable  $\alpha\text{-Al}_2\text{O}_3$  in the present combinatorial library. Indeed, none of the cast alloys are able to form external  $\alpha\text{-Al}_2\text{O}_3$  scale. While the cast alloys have higher Cr contents than the combinatorial samples in this library, and it is

	CoO	CoO	CoO
	CoCr <sub>2</sub> O <sub>4</sub>	CoCr <sub>2</sub> O <sub>4</sub>	CoCr <sub>2</sub> O <sub>4</sub>
	†CoWO <sub>4</sub>	†CoWO <sub>4</sub>	
	CoTa <sub>2</sub> O <sub>6</sub>		CoTa <sub>2</sub> O <sub>6</sub>
	†WO <sub>2</sub>		
	CrWO <sub>4</sub>	CrWO <sub>4</sub>	CrWO <sub>4</sub>
		CoTa <sub>2</sub> O <sub>6</sub>	
	CoAl <sub>2</sub> O <sub>4</sub>	CoAl <sub>2</sub> O <sub>4</sub>	CoAl <sub>2</sub> O <sub>4</sub>
	CoCr <sub>2</sub> O <sub>4</sub>	CoCr <sub>2</sub> O <sub>4</sub>	CoCr <sub>2</sub> O <sub>4</sub>
	*Cr <sub>2</sub> O <sub>3</sub>	*Cr <sub>2</sub> O <sub>3</sub>	*Cr <sub>2</sub> O <sub>3</sub>
	*AlTaO <sub>4</sub>	*AlTaO <sub>4</sub>	*AlTaO <sub>4</sub>
	Al <sub>2</sub> O <sub>3</sub>	Al <sub>2</sub> O <sub>3</sub>	Al <sub>2</sub> O <sub>3</sub>
	Alloy	Alloy	Alloy
	3-1B	3-12A	3-1L

Figure 8: Order of thermodynamically favorable oxides with increasing oxygen potential (from bottom to top) in select combinatorial compositions at 0 K, calculated from first principles. Alloy phases calculated with less than 5 % phase fraction are marked (\*), and phases calculated to not be present in all compositions are highlighted in orange and marked (†). Samples 3-12A and 3-1L have similar Ni:Co ratios, and samples 3-1B and 3-1L have lower Al content than 3-12A.

known that higher Cr contents promote oxidation resistance as noted earlier, the extent of the Cr influence on oxidation behavior is under investigation via the related combinatorial library based on cathodes 1, 2 and 3.

Beyond the potential for forming alumina, it is of interest to assess the expected formation of other oxides that may promote (or more likely interfere), with the formation of the alumina scale. Because the Ni:Co ratio and Al contents of the three cast alloys fall within the ranges explored by the present combinatorial library, one can then compare the thermodynamic predictions for the layered scales with those observed experimentally. The oxide layer ordering predicted in Figure 8 is qualitatively consistent with that observed experimentally in the cast alloys. Notably,  $\alpha$ -Al<sub>2</sub>O<sub>3</sub> is found to be the most thermodynamically favorable oxide to form on  $\gamma$ - $\gamma'$  alloys regardless of Co:Ni ratio or Al content, although the alumina formation was internal. Only certain layers of those predicted were actually observed in the cast alloy scales. Notably, AlTaO<sub>4</sub> was not observed, presumably because this phase was only calculated to be present at small (< 5 %) phase fractions. Additionally, there is also no predicted Ni content in the phases, in contrast with the experimental observations. This discrepancy is most likely a result of the absence of configurational entropy contributions in the calculations because of the implicit assumption of no solubility at 0 K. Further modeling efforts will be aimed at incorporating temperature and solubility effects in the phase stability. For example, a cluster expansion technique combined with Monte Carlo simulations can be used to incorporate the effects of configurational entropy.

Beyond the thermodynamic effects, it is evident that kinetics play a paramount role in determining whether an alloy forms the desired  $\alpha$ -Al<sub>2</sub>O<sub>3</sub> as an external scale or as an internal oxide, which is non-protective, as well as which other oxides do form in the scale. This kinetic influence is apparent in the samples oxidized for times less than 1 h (Figure 4), where internal alumina particles are observed to nucleate and remain discrete and form an IOZ underneath other external oxides. It is possible that the development of non-protective external oxides formed in addition to alumina may alter the mechanisms and kinetics of scale formation and disrupt the process of forming the continuous  $\alpha$ -Al<sub>2</sub>O<sub>3</sub> scale. Cross-section analysis of oxides grown on the three cast alloys reveals a W-rich oxide enveloping alumina particles in the IOZ of the Co-3 alloy. Such an inward-growing oxide may have the potential to disrupt external scale growth, however Co-1 and Co-2 both exhibit internal oxidation without the presence of this inward-growing oxide phase. This implies that the differentiating factor between internal and external alumina formers in the presence of other competing oxides requires a more comprehensive analysis that will be undertaken in future work.

The compositional regions of Co-base alloys with alumina scale forming behavior elucidated in this work and future publications will be compared with the location of the  $\gamma$ - $\gamma'$  two-phase field. This will define the design space of possible Co-base high temperature alloys for aerospace applications, and allow further desirable properties to be subsequently investigated, such as resistance to cyclic oxidation, water vapor, and hot corrosion attack.

## Conclusions

1. Co-base  $\gamma$ - $\gamma'$  alloys that form alumina scales in air at 1100 °C are feasible within the composition space investigated.
2.  $\alpha$ -Al<sub>2</sub>O<sub>3</sub> is predicted to be the most thermodynamically stable oxide across all Co-W-Al  $\gamma$ - $\gamma'$  compositions. Because of kinetic factors, however, it may form as an undesirable, non-protective assemblage of internal alumina particles within the metal rather than as a continuous, protective scale.
3. The combinatorial experiments revealed that external alumina scale formation in alloys with  $\sim 7$   $\mu$ m grain size occurs in compositions of xCo-yNi-zAl-10W-2Cr-3.5Ta at. %, where the ratio y/x is  $\geq 0.46$ , and z is  $\geq 10.4$  at. %

## Acknowledgments

This investigation was sponsored by the National Science Foundation under the DMREF initiative (Grant DMR 1534264). The research made use of the MRL Shared Experimental Facilities supported by the MRSEC Program of the NSF under Award No. DMR 1121053; a member of the NSF-funded Materials Research Facilities Network (www.mrnf.org). Thanks are also due to GE Global Research, especially Dr. Don Lipkin and Messrs. Scott Weaver, and Vince Tur for providing technical guidance and for performing the IPD synthesis of the combinatorial libraries. The authors are also grateful to Dr. Stephan Kramer and Messrs. Mark Cornish, Deryck Stave, and Chris Torbet for expert technical assistance.

## References

1. H.-Y. Yan, V.A. Vorontsov, D. Dye, "Effect of Alloying on the Oxidation Behavior of Co-Al-W Superalloys", *Corrosion Science*, 83 (2014), 382-395.
2. M.S. Titus, A. Suzuki, T.M. Pollock, "High Temperature Creep of New L1<sub>2</sub>-Containing Cobalt-base Superalloys", *Superalloys 2012*, ed. E.S. Huron et al. (Warrendale, PA: The Minerals, Metals and Materials Society, 2012), 823-832.
3. J. Sato et al., "Cobalt-Base High-Temperature Alloys", *Science*, 312 (2006), 90-91.
4. T.M. Pollock et al., "New Co-based  $\gamma$ - $\gamma'$  High-Temperature Alloys", *JOM*, 62 (2010), 58-63.
5. A. Suzuki, G.C. DeNolf, T.M. Pollock, "Flow Stress Anomalies in  $\gamma/\gamma'$  Two-Phase Co-Al-W-Base Alloys", *Scripta Materialia*, 56 (2007), 385-388.
6. M. Tsunekane, A. Suzuki, T.M. Pollock, "Single-Crystal Solidification of New Co-Al-W-Base Alloys", *Intermetallics*, 19 (2011), 636-643.
7. Roger C. Reed, *The Superalloys Fundamentals and Applications* (New York, NY: Cambridge University Press, 2006), 19.
8. A.G. Evans, D.R. Clarke, C.G. Levi, "The Influence of Oxides on the Performance of Advanced Gas Turbines", *Journal of the European Ceramic Society*, 28 (2008), 1405-1419.
9. A.M. Beltran, "The Oxidation and Hot-Corrosion Resistance of Cobalt-Base Superalloys", *Cobalt*, 46 (1970), 3.
10. F.H. Stott, G.C. Wood, J. Stringer, "The Influence of Alloying Elements on the Development and Maintenance of Protective Scales", *Oxidation of Metals*, 44 (1995), 113-145.
11. L. Klein et al., "Effect of B and Cr on the High Temperature Oxidation Behavior of Novel  $\gamma/\gamma'$ -Strengthened Co-Base Superalloys", *Corrosion Science*, 53 (2011), 2713-2720.
12. K. Shinagawa et al., "Phase Equilibria and Microstructure on  $\gamma'$  Phase in Co-Ni-Al-W System", *Materials Transactions*, 49 (2008), 1474-1479.
13. T. Omori et al., "Partition Behavior of Alloying Elements and Phase Transformation Temperatures in Co-Al-W-Base Quaternary Systems", *Intermetallics*, 32 (2013), 274-283.
14. L. Klein et al., "The Effect of Grain Boundaries on High Temperature Oxidation of New  $\gamma'$ -Strengthened Co-Al-W-B Superalloys", *Corrosion Science*, 79 (2014), 29-33.
15. R.R. Adharapurapu et al., "A Combinatorial Investigation of Palladium and Platinum Additions to  $\beta$ -NiAl Overlay Coatings", *Acta Materialia*, 77 (2014), 379-393.
16. D.M. Lipkin, D.R. Clarke, "Measurement of the Stress in Oxide Scales Formed by Oxidation of Alumina-Forming Alloys", *Oxidation of Metals*, 45 (1996), 267-280.
17. G. Kresse, J. Furthmuller, "Efficiency of Ab-Initio Total Energy Calculations for Metals and Semiconductors Using a Plane-Wave Basis Set", *Computational Materials Science*, 6 (1996), 15-50.
18. G. Kresse, D. Joubert, "From Ultrasoft Pseudopotentials to the Projector Augmented-Wave Method", *Physical Review B*, 59 (1999), 1758.
19. J. P. Perdew, K. Burke, M. Ernzerhof, "Generalized Gradient Approximation Made Simple", *Physical review letters*, 77 (1996), 3865.
20. G. Kresse, J. Furthmuller, "Efficient Iterative Schemes for Ab Initio Total-Energy Calculations Using a Plane-Wave Basis Set", *Physical Review B*, 54 (1996), 11169.
21. A. Jain et al., "The Materials Project: A materials genome approach to accelerating materials innovation", *APL Materials*, 1 (2013), 01102.
22. M. Kinoshita, W.D. Kingery, H.K. Bowen, "Phase Separation in NiO-CoO Solid Solution Single Crystals", *Journal of the American Ceramic Society*, 56 (1973), 398-399.
23. M. Mironova-Ulmane et al., "Raman Scattering in Nanosized Nickel Oxide NiO", *Journal of Physics: Conference Series*, 93 (2007), 012039.
24. W. Zhao et al., "Quantitative Approach for Determining the Critical Volume Fraction for the Transition from Internal to External Oxidation", *Oxidation of Metals*, 83 (2015), 187-201.
25. G. Gesmundo, F. Viani, "Transition from Internal to External Oxidation for Binary Alloys in the Presence of an Outer Scale", *Oxidation of Metals*, 25 (1986), 269-282.
26. M.P. Brady, B. Gleeson, I.G. Wright, "Alloy Design Strategies for Promoting Protective Oxide-Scale Formation", *Journal of the Minerals Metals & Materials Society*, 52 (2000), 16-21.